

From Fano-like interference to superscattering with a single metallic nanodisk

Cite this: *Nanoscale*, 2014, 6, 9093Weiwei Wan,^{†ab} Wenwei Zheng,^{†c} Yanfeng Chen^a and Zhaowei Liu^{*bd}

Superscattering was theoretically proposed to significantly enhance the scattering cross-section of a subwavelength nanostructure, far exceeding its single-resonance limit by employing resonances of multiple plasmonic modes. By numerical simulation, we design a subwavelength nanodisk as a simple candidate to achieve superscattering. Due to the phase retardation, the subradiant mode can be excited and interact with the superradiant mode in both spatial and frequency domains. By changing the height and diameter of the nanodisk, we show high tunability of the mode interaction and evolution of the resulting spectral features from Fano-like resonance to superscattering. A model of two-driven coupled oscillators is proposed to quantitatively analyze the spectral evolution. We find that the evolution is caused by not only alignment of the resonant wavelengths of related plasmonic modes, but also reasonably high loss. We show that superscattering doubles the near-field intensity, potentially enhancing the signal 16 times for SERS and 4 times for SEIRS, and doubles the far-field intensity and decreases the peak linewidth, improving the figure of merit for plasmonic refractometric sensing. Our study provides quantitative physical insight into understanding superscattering and Fano-like resonances in a single nanoparticle.

Received 18th April 2014
Accepted 26th May 2014

DOI: 10.1039/c4nr02107j

www.rsc.org/nanoscale

1. Introduction

Understanding the interaction between optical radiation and individual subwavelength objects is fundamentally important for the study of nanophotonics. It is also practically crucial for various applications such as imaging, cloaking, optical nano-antennas, and nanoplasmonic sensing.^{1–4} The scattering cross-section, which is defined by integrating the total amount of scattered power over the intensity of the incident plane wave, is usually used to describe the strength of the interaction between an object and the incident light.^{5,6} Fan and co-workers proposed that the total scattering cross-section of subwavelength structures can far exceed the single-resonance limit when constructive resonances of multiple plasmonic modes are spectrally aligned, which they term as superscattering.⁶ They have numerically demonstrated superscattering with plasmonic dielectric layered structures.^{6–8} Moreover, using two-slit

nanostructures, Fan's group theoretically demonstrated evolution of the spectral behavior from the classical analog of electromagnetically induced transparency (EIT) to superscattering, the analog of electromagnetically induced absorption (EIA), depending on excitation angles.⁸

Fano-like resonance in the plasmonic nanosystem is excited by interfering with a plasmon resonance, which acts as the broad continuum state (CS), with a narrow discrete state (DS). Depending on the different situations, the DS can be the excitation of a molecule,⁹ a diffraction channel (*e.g.*, gratings¹⁰ or plasmonic crystals¹¹), a dark plasmon mode,¹² or a guided mode.¹³ The classical analog of EIT and EIA represents special cases of the Fano-like resonance when the resonant frequencies of the involved CS and DS are almost equal.^{8,14,15} Superscattering (or EIA), EIT, and Fano-like resonance in the plasmonic system are receiving significantly growing attention because they can be used to design new materials with a controlled response to light at nanometer scales.^{12,16–19} They also provide new insights into ultrasensitive nanoplasmonic sensing²⁰ (*e.g.* surface enhanced Raman spectroscopy (SERS),²¹ localized surface plasmon resonance (LSPR) (or refractometric plasmonic sensing), and surface-enhanced IR absorption (SEIRA) spectroscopy^{9,22,23}) and interactions of plasmonic systems with sharp resonances in atoms, molecules, and quantum dots.

Most of the proposed plasmonic nanostructures for the Fano-like resonances, EIT, and superscattering (or EIA) involve the interaction of localized plasmon modes of multiple metallic particles and subcomponents.^{24–36} Therefore, they usually

^aNational Laboratory of Solid State Microstructures and Department of Materials Science and Engineering, Nanjing University, Nanjing, 210093, People's Republic of China

^bDepartment of Electrical and Computer Engineering, University of California, San Diego, 9500 Gilman Drive, La Jolla, California, 92093, USA. E-mail: zhaowei@ucsd.edu

^cDepartment of Physics, University of California, San Diego, 9500 Gilman Drive, La Jolla, California, 92093, USA

^dMaterials Science and Engineering, University of California, San Diego, 9500 Gilman Drive, La Jolla, California, 92093, USA

[†] These authors contributed equally.

require stringent design and precise control of the arrangement of individual components such as inter-particle distance and particle shape, which impose experimental difficulties. To the best of our knowledge, only López-Tejiera *et al.* theoretically demonstrate the Fano-like interference of plasmon resonances at a single rod-shaped nanoantenna with adjacent modes partially overlapping in both frequencies and space, giving rise to the interaction (or non-orthogonality) between them.^{37,38} However, they only explore the interference of longitudinal plasmonic modes of the nanorod, leading to the limit geometrical control of the mode interactions. In most reported studies of plasmonic Fano-like resonance,^{24–36} the dark mode is not excited directly by light, but excited indirectly by the near-field coupling with the bright mode. Therefore, the model of one-driven coupled oscillators is generally applied for the quantitative analysis. The two-driven coupled oscillators model described by Luk'yanchuk is believed to have improved accuracy and generality for modelling coupled resonant systems,²⁴ but no specific plasmonic Fano-resonated nanostructures were proposed by this classic analog.

Here we present a single metallic nanodisk to achieve superscattering. Compared to the layered structures, the single nanodisk is a simple plasmonic structure, resulting in an enhanced near field that is fully accessible for SERS,^{39–41} SEIRA,^{20,42,43} and other surface-enhanced spectroscopic processes.^{44,45} We also observe that a nanodisk can exhibit evolution of the spectral feature from Fano-like resonance to superscattering (or EIA) by adjusting its diameter or height, showing high tunability. Because the subradiant modes can be excited by the phase retardation,^{20,46,47} a model of two-driven coupled oscillators is used to quantitatively analyze this evolution process. We find that the evolution is caused by not only alignment of the resonant wavelengths of related plasmonic modes, but also reasonably high loss. We show that the superscattering of the nanodisk can improve not only the signal-to-noise ratio of the spectral extinction and the surface enhanced vibrational spectra due to the enhancement of both far field and near field intensity, but also the figure of merit of LSPR sensing about two times due to the narrower resonance linewidth.

2. Simulation section

The nanodisk we propose is shown in Fig. 1. All sharp corners of the nanodisk have been slightly smoothed out by cylindrical surfaces with a radius of 5 nm to avoid unphysical structural discontinuities, mimicking a nanodisk that can be fabricated in practice. To demonstrate the evolution from Fano-like resonance to superscattering, the height is varied from 30 to 120 nm with the diameter fixed at 80 nm or the diameter from 40 to 100 nm with the height fixed at 60 nm. The finite integration time domain (FITD) solver of the CST® microwave studio is used to obtain both the far-field spectra (*e.g.* absorption, scattering, and extinction spectra) and the near-field spectra of all the nanodisks. The scattering and absorption cross-section was computed by the built-in functions that integrate the total amount of power scattered and absorbed by the nanodisk over

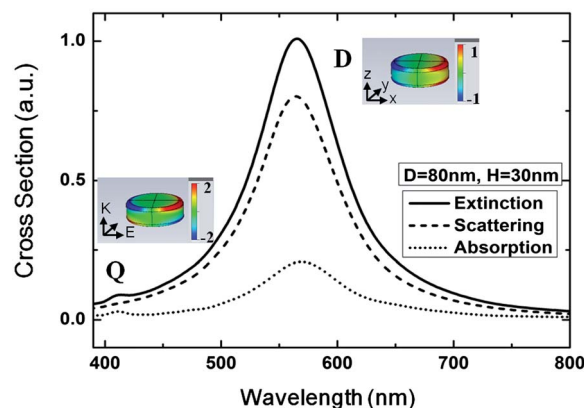


Fig. 1 FITD simulation of the extinction (solid line), scattering (dashed line), and absorption spectra (dot line) for a silver nanodisk with a diameter of 80 nm and a height of 30 nm in the surrounding media of the refractive index 1.4 when the nanodisk is illuminated by a normal incident plane wave with propagation in the *z* direction and polarization in the *x* direction. Two insets are the charge distributions normalized by $5 \times 10^{-11} \text{ C m}^{-2}$ at the resonant wavelengths of the Q mode (408 nm) and the D mode (560 nm), respectively.

the intensity of the incident plane wave, respectively. The extinction is the sum of them. The finite element (FEM) frequency domain solver of the CST® microwave studio is used to calculate the charge distributions at the resonance wavelength identified by the far-field spectra. The nanodisk is made of silver immersed in uniform surrounding media with a refractive index of 1.4 (*e.g.* polydimethylsiloxane (PDMS)). To describe materials properties of silver, the experimentally fit Drude model⁴⁸ was used with

$$\varepsilon_r(\omega) = \varepsilon_\infty - \frac{\omega_p^2}{\omega(\omega + i\gamma_c)}, \quad (1)$$

where ε_∞ is 4, ω_p is $1.336 \times 10^{16} \text{ rad s}^{-1}$, and γ_c is $1.108 \times 10^{14} \text{ rad s}^{-1}$. The illumination is normal to the bottom surface of the nanodisk and the polarization is along the diameter of the nanodisk (*x*-polarization). All other boundaries is set to be open with perfectly matched layers (PML) to absorb all outgoing radiation and eliminate any reflection at the boundaries.

3. Results and discussion

3.1 Uncoupled plasmonic modes

To understand the origin of Fano-like resonance and superscattering in the single nanodisk, we first consider a single silver nanodisk with a diameter of 80 nm and a height of 30 nm that exhibits the nearly uncoupled superradiant and subradiant modes. In Fig. 1, two peaks with little spectral overlap appear at 560 nm and 408 nm, respectively, in the absorption spectrum. This result indicates the existence of two localized plasmonic modes that are supported by the corresponding charge distributions of the nanodisk at two peak frequencies: when the resulting top dipole and bottom dipole of the nanodisk are close, they interact and form two new hybridized modes. According to the plasmon hybridization theory,^{20,49} those two

hybridized modes are termed a superradiant mode (bright dipolar mode, D), the lower-energy “bonding” mode, and a subradiant mode (dark quadrupolar mode, Q), the higher-energy “antibonding” mode. The validity of the hybridization model is supported by the surface charge distribution analysis of the D and Q modes at their resonant frequencies. A simple way of visualizing the charge density is to compute the normal component of the electric displacement at the material interface of the single silver nanodisk that is directly equal to the surface charge density according to the boundary conditions. From the corresponding insets of Fig. 1, we see that the related mode profiles are expected from the hybridization diagram: the D mode shows in-phase oscillation of both dipoles at the top and bottom of the nanodisk, generating a large total dipole moment which makes the mode highly radiative and the Q mode possesses zero net dipole moment because of the out-of-phase alignment of the dipoles and is subradiant. The little spectral overlap of these two modes in the adsorption spectrum indicates nearly no coupling between them because the incident light with a wavelength of 560 nm has high efficiency to excite the D mode and near zero efficiency to excite the Q mode and similarly for the light with a wavelength of 408 nm. Although the Q mode can be excited by the phase retardation,⁵⁰ the vanishing radiative efficiency results in the indiscernible peak in the scattering spectrum and the Q mode can only be found in the absorption spectrum with narrower bandwidth. The extinction spectra of Q mode are much narrower than the one of D mode because the Q mode has intrinsic non-radiative loss, but much lower radiative loss.⁵¹

3.2 Fano-like resonance and superscattering

With the knowledge of the uncoupled D and Q modes, we then examine single silver nanodisks with the same diameter of 80 nm as the one in Fig. 1, but with various heights that have the strongly coupled D and Q modes: one with a height of 60 nm shows Fano-like resonance (Fig. 2a–g) and the other with a height of 120 nm exhibits superscattering (Fig. 2h–m). Generally, an uncoupled resonance is characterized by a phase (φ_R) that matches the phase of the incident field ($\varphi_R = 0$) on one side of the resonance and is out-of-phase on the other side ($\varphi_R = \pi$).⁵² At the frequencies in between, the phase transits from 0 to π . The higher the loss of the resonance is, the more slowly the phase transits, and the wider the transition region is. In the coupled systems under study, when both D and Q modes are excited and their resonances come close, the absolute difference of their phase ($|\varphi_d - \varphi_q|$ or $|\Delta\varphi|$) is between 0 and 0.5π in some regions of the spectrum, forming a stronger resonant mode because of constructive interference. The closer to 0 the absolute phase difference is, the more constructive the interference is. On the other hand, in the spectral region where $|\Delta\varphi|$ is between 0.5π and π , a weaker mode is formed because of destructive interference. The closer to π the absolute difference is, the more destructive the interference is. When $|\Delta\varphi|$ is equal to 0.5π at some frequency, the D and Q modes do not interfere, which is termed orthogonality. The dip that characterizes the Fano-like resonance in Fig. 2a arises from the destructive

interference of the D and Q modes that overlap spectrally and spatially. However, the Fano-like resonance in single nanodisks can disappear in two extreme cases. One is that the D and Q modes resonate at the frequencies so far away from each other that one mode can hardly be excited at the excitation wavelength of the other mode as shown in Fig. 1. The other is that two modes resonate at the frequencies so close that they can interfere constructively during their whole spectral range. This extreme case is termed superscattering^{6–8} as shown in Fig. 2h, where the peak intensity of the extinction spectrum increases about twice than the one in Fig. 2a.

The underlying mechanism of the Fano-like resonance and superscattering is also supported and further understood by analyzing the FEM simulated charge distribution and near-field of the plasmon modes that appear at specific frequencies as shown in Fig. 2(b–g) and (i–m), respectively. From Fig. 2c, we see that the D and Q modes interfere destructively, forming the corresponding mode profile at the Fano-like resonance of 472 nm, termed the D – Q mode. The D – Q mode has the surface charge concentrated at the top two corners of the nanodisk, leading to the co-localized near-field intensity as shown in Fig. 2f. Interestingly, from Fig. 2b and d, the distribution of the surface charge at the peaks surrounding the Fano-like resonance is dominated by the Q and D modes, respectively. Fig. 2e and g reveal the expected related near-field distribution: both the related near-field distributions of the Q and D modes are localized at the four corners of the nanodisk. This shows that although the geometry of single nanostructure can enable the D and Q modes to strongly interact with each other, the D and Q modes can be dominantly excited at specific wavelengths. This finding, which has been recently shown for the multi-element nanosystems (*e.g.* the nanoantenna arrays⁵³ and assemblies of nanorods and nanoantennas¹⁶), is important because it enables a detailed spatial tuning of the near-field with frequency at the nanoscale. Our work represents a significant step forward by demonstrating the selective excitation of different parts inside a single-element strongly coupled nanosystem (Fig. 2b–d). From Fig. 2i–l, we observe that the superscattering nanodisk is characterized by the dual-mode character (D, Q, D + Q, and D – Q) at different phases of the charge-oscillation period. The related near field in Fig. 2m at the four corners of the nanodisk is stronger than the ones of the Q and D modes in Fig. 2e and g because two modes interfere constructively in the superscattering nanodisk.

3.3 Modelling by two-driven coupled oscillators

To obtain better physical insights of Fano-like resonance and superscattering in a single silver nanodisk, we apply a model of two-driven coupled oscillators (TCO) (Fig. 3a).²⁴ Each of the oscillators is driven by the incident harmonic field $\vec{E}_0 = E_0 e^{-i\omega t}$. Two driven oscillators simulate the related charge oscillations of the D mode (excited by the direct coupling of the incident light) and Q mode (resulted from the phase retardation). They are coupled with the coefficient κ and are characterized by resonant frequencies ω_d and ω_q , loss γ_d and γ_q , and excitation coefficients g_d and g_q . The equations of

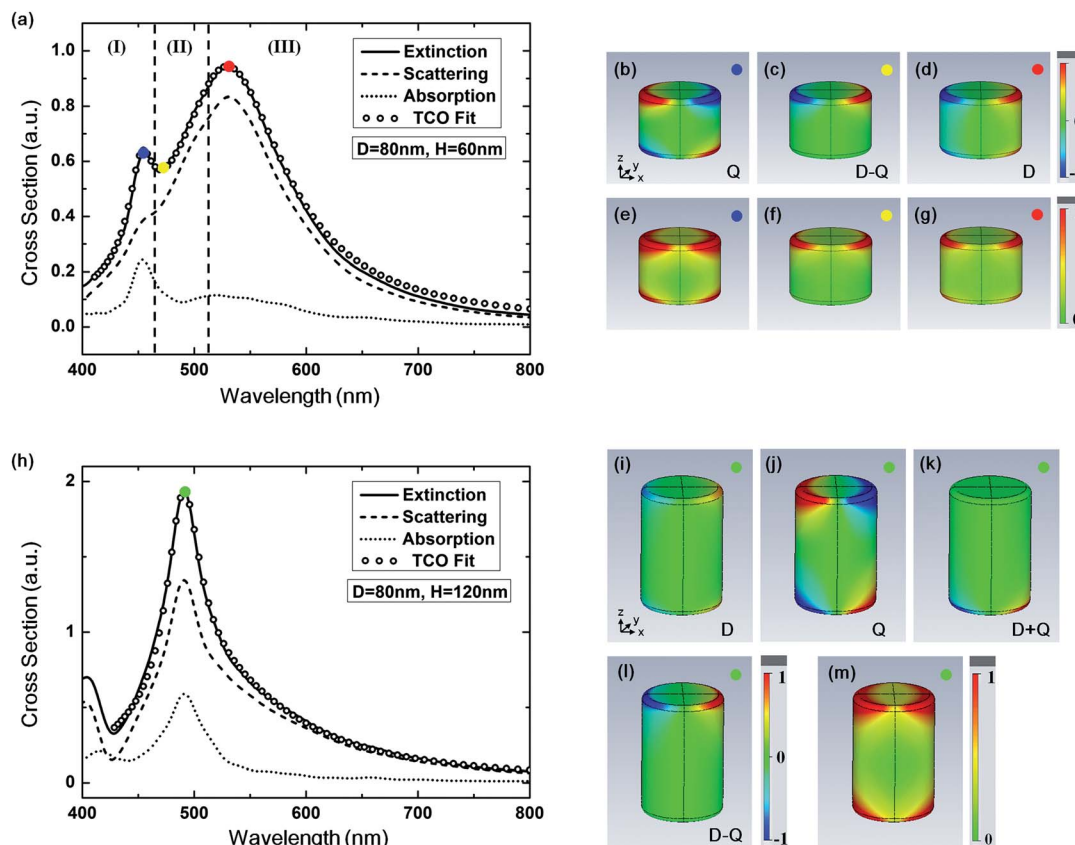


Fig. 2 (a) FITD simulation of the extinction (solid line), scattering (dashed line), and absorption spectra (dot line) for a silver nanodisk with a diameter of 80 nm and a height of 60 nm that exhibits typical Fano-like resonance. The curve of circles represents the two-drive coupled oscillators (TCO) model fit of the extinction spectrum. (b–d) FEM simulation of the surface charge distribution normalized by $2.5 \times 10^{-10} \text{ C m}^{-2}$ at the selected wavelengths shown in (a): 455 nm (the blue dot, the Q mode), 472 nm (the yellow dot, the D – Q mode), and 531 nm (the red dot, the D mode). (e–g) The related average $|E|$ field normalized by 10 V m^{-1} . (h) FITD simulation of the various cross-sections for a silver nanodisk with a diameter of 80 nm and a height of 120 nm that exhibits typical superscattering. (i–l) FEM simulation of the surface charge distribution normalized by $2.5 \times 10^{-10} \text{ C m}^{-2}$ at a peak wavelength of 492 nm shown in (h) (green dots) at different phases of one charge-oscillation period, showing the characteristics of the D, Q, D + Q, and D – Q modes. (m) The related average $|E|$ field normalized by 10 V m^{-1} . (For all the FITD and FEM simulation, the surrounding media have a refractive index of 1.4 and the nanodisk is illuminated by a normal incident plane wave with propagation in the z direction and polarization in the x direction.). Note: the surface charge distribution of the D, Q, D + Q, and D – Q modes is characterized as follows: the D and Q modes have the charge confined at the four corners of a nanodisk symmetrically and asymmetrically, respectively, and the D + Q and D – Q modes have the charge confined at the bottom and top two corners of a nanodisk, respectively, assuming that the light comes from the bottom of the nanodisk.

motion can be solved in terms of transient charge displacement x_d, x_q from the equilibrium positions:

$$\begin{aligned} \ddot{x}_d + \gamma_d \dot{x}_d + \omega_d^2 x_d - \kappa x_q &= g_d E_0 e^{-i\omega t}, \\ \ddot{x}_q + \gamma_q \dot{x}_q + \omega_q^2 x_q - \kappa x_d &= g_q E_0 e^{-i\omega t}. \end{aligned} \quad (2)$$

This model has general validity, and under specific conditions, *i.e.* when $g_q = 0$, the TCO model converges to the simpler single driven coupled oscillators model that simulates the multi-element plasmonic nanosystems:^{15,24,52,54,55} the light excites only the broad mode, *e.g.* x_d , while the narrow resonance mode x_q (dark mode) is excited only due to the near-field coupling. The steady state solutions of eqn (2) are also harmonic and given by²⁴

$$\begin{aligned} x_d(t) &= C_d(\omega) e^{-i\omega t} \\ &= \frac{g_q \kappa + g_d (\omega_q^2 - \omega^2 - i\gamma_q \omega)}{(\omega_d^2 - \omega^2 - i\gamma_d \omega)(\omega_q^2 - \omega^2 - i\gamma_q \omega) - \kappa^2} e^{-i\omega t}, \\ x_q(t) &= C_q(\omega) e^{-i\omega t} \\ &= \frac{g_d \kappa + g_q (\omega_d^2 - \omega^2 - i\gamma_d \omega)}{(\omega_d^2 - \omega^2 - i\gamma_d \omega)(\omega_q^2 - \omega^2 - i\gamma_q \omega) - \kappa^2} e^{-i\omega t}. \end{aligned} \quad (3)$$

The transient energy loss of the incident light due to the D and Q modes is

$$\begin{aligned} P_d(t) &= g_d e^{-i\omega t} \dot{x}_d(t), \\ P_q(t) &= g_q e^{-i\omega t} \dot{x}_q(t), \end{aligned} \quad (4)$$

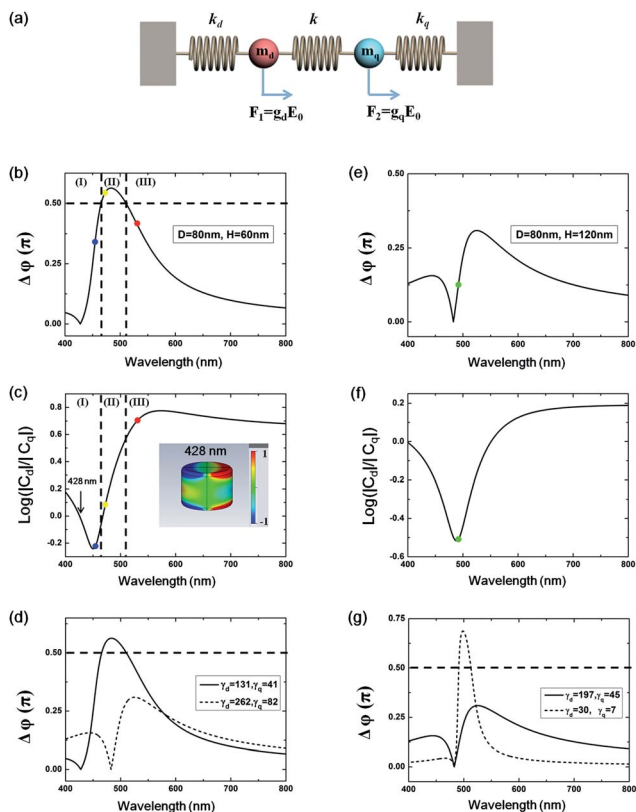


Fig. 3 (a) Schematic of the two coupled oscillators (TCO) model proposed to fit all the extinction spectra of single nanodisks. (b) $|\varphi_d - \varphi_q|$ ($|\Delta\varphi|$) for the nanodisk with a diameter of 80 nm and a height of 60 nm featured by the Fano-like resonances (Fig. 2a). (c) The related logarithmic scale of the absolute ratios of $|C_d|$ over $|C_q|$ ($|C_d|/|C_q|$), with $|C_d|/|C_q| = 5.1$ for the D mode at 531 nm (red dot), $|C_d|/|C_q| = 1.2$ for the D – Q mode at 472 nm (yellow dot), and $|C_q|/|C_d| = 1.7$ for the Q mode at 455 nm (blue dot). The inset shows the FEM simulated surface charge distribution (normalized by $3 \times 10^{-11} \text{ C m}^{-2}$) of the composite mode excited at a wavelength of 428 nm that contains the higher-order mode. (d) The related spectra of $|\Delta\varphi|$ under the increased hypothetical loss, evolving the spectral features from the Fano-like resonances shown in Fig. 3b (solid lines) to superscattering (dashed line). (e–g) The same parameters as the ones in (b–d), respectively, but for the nanodisk with a diameter of 80 nm and a height of 120 nm featured by the superscattering (Fig. 2h).

The corresponding energy loss averaged over one period is

$$P_d(\omega) = \frac{2\pi i \omega [g_d g_q \kappa + g_d^2 (\omega_q^2 - \omega^2 - i\gamma_q \omega_q)]}{(\omega_d^2 - \omega^2 - i\gamma_d \omega)(\omega_q^2 - \omega^2 - i\gamma_q \omega) - \kappa^2}, \quad (5)$$

$$P_q(\omega) = \frac{2\pi i \omega [g_d g_q \kappa + g_q^2 (\omega_d^2 - \omega^2 - i\gamma_d \omega_d)]}{(\omega_d^2 - \omega^2 - i\gamma_d \omega)(\omega_q^2 - \omega^2 - i\gamma_q \omega) - \kappa^2}.$$

Therefore, the sum of P_d and P_q is the total energy loss $P_t(\omega)$ of the incident plane wave due to the plasmonic response of the nanodisk. The real part of $P_t(\omega)$ is then used to model the extinction spectrum of the nanodisk.^{54–56} A fit of the extinction spectra of Fano-like resonance and superscattering in Fig. 2a and h is shown with the circles, showing excellent agreement with the FITD results.

The complex amplitude $C_{d,q}(\omega)$ in eqn (3) can also be written as

$$C_{d,q}(\omega) = |C_{d,q}(\omega)| e^{-i\varphi_{d,q}(\omega)}, \quad (6)$$

where the amplitude is $|C_{d,q}(\omega)|$ and the phase is $\varphi_{d,q}(\omega)$, providing information on the frequency response of the system. As mentioned previously, we can now use the absolute phase difference between these two modes ($|\varphi_d - \varphi_q|$ or $|\Delta\varphi|$) to quantitatively evaluate the interference between the D and Q modes: $|\Delta\varphi|$ of 0.5π shows orthogonal interference, $|\Delta\varphi|$ between 0 and 0.5π indicates constructive interference, and $|\Delta\varphi|$ between 0.5π and π shows destructive interference. Fig. 3(b–d) and (e–g) show how different excitation wavelengths affect $|\Delta\varphi|$, and the logarithmic scale of the ratios of $|C_d|$ over $|C_q|$ ($\log(|C_d|/|C_q|)$) for the nanodisks featured by the Fano-like resonance and superscattering in Fig. 2a and h, respectively. Regarding the nature of the mode interference determined by $|\Delta\varphi|$, we divide Fig. 2b and 3b and c into the following regions: Region I, III represents constructive interference of both modes while Region II represents destructive interference. Moreover, in all the figures, we use the circles of the same color to label the resonant wavelengths of the D, D – Q, Q modes and the superscattering. All the parameters extracted from the TCO model fit (Fig. 3 and Tables 1 and 2) add the quantitative physical insight into the previous qualitative analysis of the features (modes and peaks) of both the Fano-like resonance and superscattering as follows. From Fig. 3b and c for the Fano-like resonance (Fig. 2a), we find that the D – Q mode of the Fano-like resonance requires that both the D and Q modes interfere destructively, but also have the comparable absolute amplitude ($|C_d|/|C_q|$ of 1.2 shown in Fig. 3c). Interestingly, at the resonance wavelengths of the D (red dot) and Q modes (blue dot), $|\Delta\varphi|$ is less than 0.5π with $|C_d|/|C_q|$ of 5.1 and $|C_q|/|C_d|$ of 1.7 as shown in Fig. 3c, respectively. This indicates that the dominant feature of the D or Q mode is caused by one mode being excited much more effectively than the other mode at the related resonance wavelength. $|\Delta\varphi|$ changes gradually toward 0 at both the blue and red ends of the spectra as shown in Fig. 3b because the phases of both the D and Q modes converge to zero at the red end and π at the blue end as the wavelength is moved further away from both the resonances. A similar phenomenon occurs in Fig. 3e for the superscattering as well. In Fig. 3e, $|\Delta\varphi|$ is less than 0.5π across the spectra. This result supports that the Fano-like resonance does not occur in the extreme case of superscattering because of the lack of the destructive interference. Fig. 3c and f show how the D and Q modes relatively contribute to the spectrum intensity for the Fano-like resonance and superscattering shown in Fig. 2a and h, respectively. Generally, the Q mode is dominant at short wavelengths while the D mode is dominant at long wavelengths. With these insights, we are able to explain why the D + Q mode (with the surface charge concentrated at the bottom corners of the nanodisks) does not appear when both modes interfere constructively at Regions I and III for the Fano-like resonance in Fig. 2a as follows. In Region I longer than 428 nm and Region III, one mode at the related excitation wavelength is much

Table 1 Extracted Parameters from the TCO model for varying heights (Fig. 4a)

Height ($D = 80$ nm)	ω_d (THz)	ω_q (THz)	γ_d (THz)	γ_q (THz)	$\sqrt{\kappa}$ (THz)	g_d (THz $^{-1}$)	g_q (THz $^{-1}$)
60 nm	566	663	131	41	42	11.0	3.6
70 nm	570	648	141	41	40	11.1	4.4
80 nm	571	638	150	43	43	11.1	5.4
90 nm	574	629	167	42	42	11.3	6.1
100 nm	578	623	175	41	40	11.3	6.6
110 nm	581	617	186	41	39	11.5	7.0
120 nm	581	612	197	45	41	11.0	7.9

Table 2 Extracted parameters from the TCO model for varying diameters (Fig. 4e)

Dia. ($H = 60$ nm)	ω_d (THz)	ω_q (THz)	γ_d (THz)	γ_q (THz)	$\sqrt{\kappa}$ (THz)	g_d (THz $^{-1}$)	g_q (THz $^{-1}$)
40 nm	680	688	72	30	40	4.6	2.5
50 nm	652	675	82	33	44	6.1	2.8
60 nm	622	669	100	34	42	8.0	2.9
70 nm	594	665	110	35	41	9.3	3.3
80 nm	566	663	131	41	42	11.0	3.6
90 nm	539	657	140	48	40	12.2	4.1
100 nm	515	654	153	50	41	13.6	4.4

stronger than the other mode at the same wavelength as shown in Fig. 3c. Therefore, the D mode is still dominant in Region III while the Q mode is dominant in Region I longer than 428 nm. In Region I short than 428 nm, the high-order mode is excited and mixed with the D and Q modes, which is indicated by the exemplary surface charge distribution at 428 nm as shown in the inset of Fig. 3c.

Most interestingly, by hypothetically increasing the loss of the D and Q modes, we can evolve the Fano-like resonance in Fig. 2a to the superscattering and *vice versa* for the superscattering in Fig. 2h to the Fano-like resonance, as shown in Fig. 3d and g, respectively. The lower the loss is, the more destructively two modes interfere, the more significantly the Fano-like resonance is. The higher the loss is, the more constructively two modes interfere, the more significantly superscattering is. This is due to lower loss resonances having the faster phase transits from 0 to π . This faster transition requires that the resonance wavelengths of the two modes come closer so that they can interfere constructively across the whole spectrum to ensure the superscattering. This indicates that the evolution from Fano-like resonance to superscattering is caused by not only alignment of the resonant wavelengths of related plasmonic modes, but also reasonably high loss.

The geometry of a single nanodisk plays an important role in determining the energy of the D and Q modes and their interaction. By varying the geometry, we can tune the characteristic plasmonic responses of a silver nanodisk evolved from Fano-like resonance to superscattering through controlling resonant frequency of plasmonic modes along with their loss. In the following, we explore the tunability of the spectral features through diameter and height change of a silver nanodisk and analyze the resulting extinction spectra by the TCO model to

provide more insights into the evolution. Whenever we compare the extinction spectra of the nanodisks with different diameters (D) (e.g. study of diameter tuning), we use the ones normalized by the physical cross-section ($\pi D^2/4$) of the related nanodisk. Fig. 4a and e show how the height and the diameter affect the extinction spectra that agree excellently with the TCO model fit (solid circles). The corresponding effects on $|\Delta\phi|$ are also shown in Fig. 4b and f respectively. By increasing height or decreasing diameter, the maximum of the $|\Delta\phi|$ changes from above 0.5π to below 0.5π , indicating that the spectral feature evolves from Fano-like resonance to superscattering. The parameters are extracted from the TCO model fit as selectively shown in Fig. 4c, d, g and h and summarized in Tables 1 and 2, respectively.

As shown in Fig. 4a, the peak associated with the D mode (D peak) is blue-shifted and the peak associated with the Q mode (Q peak) is red-shifted with the height increasing. Both the shifts are quantified through the TCO fit (Fig. 4c) and are explained according to the plasmon hybridization theory²⁰ as follows: as the height increases, the top and bottom dipoles of the nanodisk interact more weakly, decreasing the stored energy of the bonding D mode (ω_d), while increasing the one of the antibonding Q mode (ω_q). As a result, the resonant frequencies of the D and Q modes come toward each other. The closer resonant frequencies combined with the increased loss γ_d and almost unchanged γ_q (Fig. 4d and Table 1) result in the spectral features evolving from Fano-like resonance to superscattering as shown in Fig. 4a and b. By contrast, Fig. 4g and Table 2 show that both ω_d and ω_q increase with decreasing diameter, which is due to the size effect along the light polarization direction.^{47,57} Moreover, ω_d increases significantly faster than ω_q , making ω_d and ω_q converge. This overlapping of ω_d and ω_q can decrease $|\Delta\phi|$. Meanwhile, Fig. 4h and Table 2 show

that both losses, γ_d and γ_q , decrease with decreasing diameter, potentially increasing $|\Delta\phi|$. However, Fig. 4f shows that $|\Delta\phi|$ decreases as diameter decreases. This decrease indicates that the quick overlapping of ω_d and ω_q dominantly affects $|\Delta\phi|$, causing the spectral feature to evolve from Fano-like resonance to superscattering as shown in Fig. 4e.

Fig. 4c and g show that ω_d is more sensitive to changes of diameter than changes of height and ω_q *vice versa*. This indicates that we can control $\omega_{d,q}$ selectively through different geometrical parameters. The result arises from different major excitation mechanisms of the D and Q modes. The Q mode is excited by the phase retardation that is sensitive to the height of the nanodisk. The D mode is excited by radiative coupling of light that is proportional to the square of the total dipole moment of the plasmons in the dipole approximation. The total dipole moment of the D mode is mainly determined by the diameter of the nanodisk while the one of the Q mode is always zero. The above explanation is supported by the excitation coefficients $g_{d,q}$: Fig. 4c and Table 1 show that g_q increases with increasing height while g_d remains almost constant, and Fig. 4g and Table 2 show the opposite with the diameter increasing. Interestingly, Tables 1 and 2 show that the coupling coefficient

between the D and Q mode is insensitive to the change of either height or diameter. This is because the excited surface charges (or E-field) of both the D and Q modes (Fig. 1, 2(b–g) and (i–m)) are concentrated around the four corners of the nanodisks regardless of either diameter or height. The result indicates that the coupling of the D and Q mode is mostly due to the spatial overlapping, which is unique in the single-element nano-system.³⁷ It is worth mentioning that although the resonance peaks of the D and Q modes could be close to each other (Fig. 4a, c, e and g), they cannot crossover with each other. This anti-crossing is consistent with the plasmon hybridization theory:²⁰ the resonance peaks of the bonding (*i.e.* D mode) and antibonding (*i.e.* Q mode) modes can asymptotically converge as the primitive un-hybridized modes interact with less and less strength.

Fig. 4d and h show that the loss γ_d of the D mode is significantly higher than the loss γ_q of the Q mode due to the significantly higher radiative loss. Moreover, γ_d increases with both the height and diameter almost linearly due to the increased dipole moments with the increasing size. Meanwhile, γ_q almost keeps constant with the increase of the height and increases slowly with the increase of the diameter. This effect may attribute to the unchanged or slightly changed overlap between materials and electromagnetic fields with various geometries.

4. Applications of superscattering in nanoplasmonic sensing

The enhanced extinction results from enhanced scattering and absorption. A silver nanodisk with the superscattering effect can be served as not only a strong scatterer for biomedical imaging, but also a strong absorber for the thermal therapy and solar cells. Moreover, due to the co-localization of the D and Q modes, the spectral overlap could enhance the near electric field. The enhanced near-field intensity is also useful to improve the sensitivity of spectroscopic techniques, such as SERS and SEIRA for the molecular detection.^{58,59} The intensity of the near electric field is monitored by the probe that is 1 nm away from the corner and represented by point A in the inset of Fig. 5a. As shown in Fig. 5a, compared to the nanodisk without the superscattering effect (*e.g.* the one with a height of 30 nm and a diameter of 80 nm), the near field of the superscattering nanodisk (*e.g.* the one with a height of 105 nm and a diameter of 80 nm) is enhanced about two times. Since the intensity of SERS is proportional to E^4 and the SEIRA is proportional to E^2 ,^{58,59} a superscattering nanodisk can potentially improve signals 16 times for SERS and 4 times for SEIRA.

Superscattering can also improve sensitivity of refractive-index sensing that is typically evaluated by the figure of merit (FoM) defined as⁶⁰

$$\text{FoM} = \frac{S(\text{nm} \times \text{RIU}^{-1})}{\Delta\lambda(\text{nm})}, S = \frac{\partial\lambda(\text{nm})}{\partial n(\text{RIU})}, \quad (7)$$

where the bulk refractive index sensitivity, S , is the ratio of the LSPR peak shift ($\partial\lambda$) per change of refractive index unit (RIU)

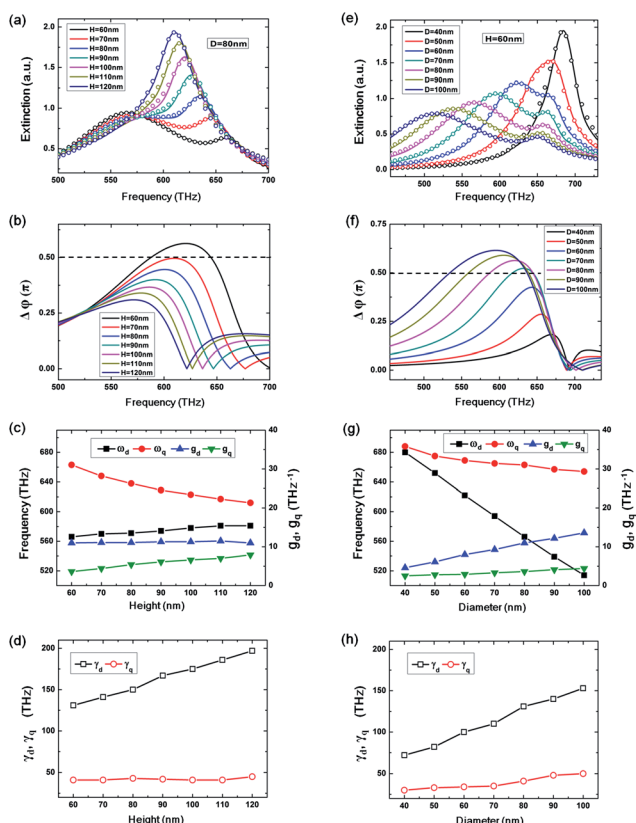


Fig. 4 (a) FITD simulation (solid curves) and the TCO model fit (circles) of the extinction spectra for the nanodisks with the diameter fixed at 80 nm and the height varied from 60 nm to 120 nm. (b) The related $|\Delta\phi|$. (c and d) extracted parameters from the TCO model fit in (a) versus the height of the nanodisks. (e–h) The same parameters as the ones in (a–d), respectively, but for the nanodisks with a height of 60 nm and the diameter varied from 40 nm to 100 nm.

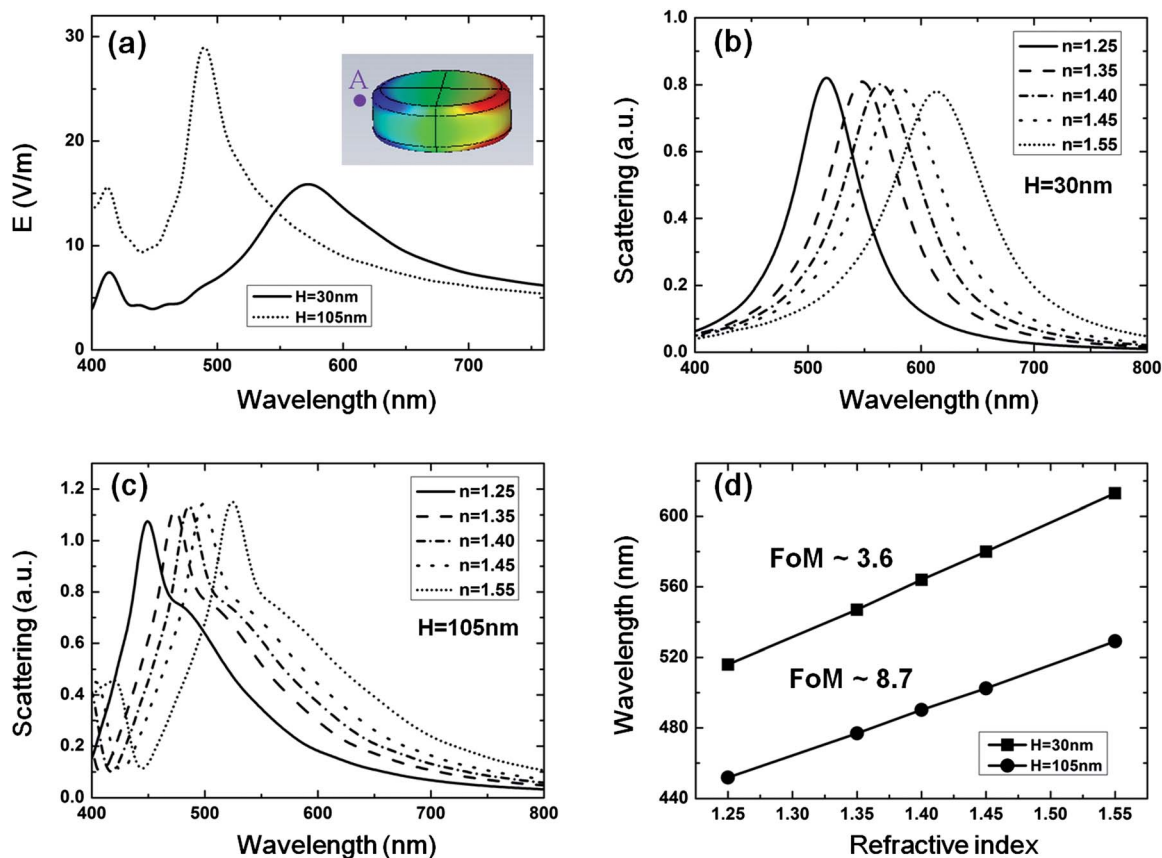


Fig. 5 Comparison of the nanodisks with 80 nm in diameter, but with the different heights of 30 nm without the superscattering effect and 105 nm with the superscattering effect on sensing performance. (a) Intensity of the near electric field measured by a FITD simulation probe at point A that is 1 nm away from the top corner of the related nanodisk. (b and c) Scattering cross-sections of the nanodisk with 30 and 105 nm in height in the surrounding media of different refractive indices (n), respectively. (d) The related figure of merit (FoM) (calculated from the TCO model fit of (b) and (c)) versus the related refractive index (n).

in the surrounding media (∂n) and $\Delta\lambda$ is the full width at half maximum (FWHM) of the spectral resonant peak. We compare sensitivity of the nanodisks with and without the superscattering effect that corresponds to the nanodisks with the same diameter of 80 nm, but with the height of 30 nm and 105 nm as shown in Fig. 5b and c, respectively. Fig. 5b and c show that the peak is broad with the increase of refractive index (n) as expected.⁴⁷ Therefore, we used the FWHM of the corresponding spectral peak for $n = 1.4$ to approximate $\Delta\lambda$ of all the spectra for the n ranged from 1.25 to 1.55. Interestingly, the scattering spectra in Fig. 5c are asymmetric because the peaks of the D and Q modes are significantly overlapped, but not exactly aligned. For example, by fitting the spectrum for $n = 1.4$ with the model of two-couple oscillators (TCO) (in the same way as shown in Fig. 2a), the resonance wavelengths for the D and Q modes are 518 and 484 nm, respectively. Because the maximum of the overlapped asymmetrical peaks dominantly come from the one for the Q mode as shown in Fig. 5c, we use the loss (γ_q) of the Q mode (obtained by the TCO fit) to obtain the FWHM of the spectrum for $n = 1.4$. Fig. 5d shows that the nanodisk with the superscattering effect (the one with 105 nm in height) increases the FoM from 3.6 to 8.7.

5. Conclusions

We present a single silver nanodisk as a simple but promising candidate to realize not only Fano-like resonance, but also superscattering. By FITD simulation, we show that because of the spatial co-localization, the Q and D modes could become non-orthogonal and interfere strongly with each other, leading to both Fano-like resonance and superscattering. Furthermore, we demonstrate that the illumination at different frequencies can selectively excite different plasmonic modes (e.g. the D, D – Q, and Q modes) with different near-field distributions within a single nanodisk even when the plasmonic modes are strongly coupled. This selective excitation enables us to spatially tune the near-field intensity with frequencies inside a single-element strongly coupled nanosystem. We then show by either increasing the height or decreasing the diameter of a nanodisk, the extinction spectral feature of the nanodisk can be evolved from Fano-like resonances to superscattering. The model of two-driven coupled oscillators is applied to quantitatively analyze the evolution. We find that the evolution is caused by not only aligning the resonance wavelengths of related plasmonic modes, but also reasonably large loss. An engineered superscattering silver nanodisk can enhance both the electric

field in far-field and near-field and decrease the linewidth of the resonance peak of interest, which is desirable and beneficial for improving the performance of various nanoplasmonic sensors.

These studies provide systematic and quantitative insights into the general electromagnetic properties of a single-element strong coupled plasmonic nanosystem. The superscattering effect of a single nanodisk can also be applied to other unsymmetrical single-elements (e.g. nanostars⁶¹ and nanotriangles^{62–64}) and multi-element plasmonic nanosystems because it exploits the phase retardation, one of the general effects arising from the size of the nanostructures. Moreover, the intra-particle mode engineering may be potentially combined with inter-particle mode engineering. This combination introduces more freedoms in the design, leading to more complex and versatile plasmonic nanosystems to achieve more superior properties. For such more complex nanosystems, the two-driven coupled oscillators model may be extended to multiple-driven multiple couple oscillators to quantitatively analyze the mode interactions and predict the spectral features. Therefore, a single metallic nanoparticle capable of both Fano-like resonance and superscattering provides a new perspective in terms of engineering the light-matter interaction at the nanoscale, which is essential for many applications such as surface-enhanced sensing and imaging.

Acknowledgements

The authors acknowledge partial financial support from NSF-ECCS under Grant # 0969405, the Gordon Moore Foundation, and the National Basic Research Program of China under Grant no. 2012CB921503 and 2013CB632702.

Notes and references

- J. Yao, M. E. Stewart, J. Maria, T.-W. Lee, S. K. Gray, J. A. Rogers and R. G. Nuzzo, *Angew. Chem., Int. Ed.*, 2008, **47**, 5013–5017.
- J. B. Pendry, D. Schurig and D. R. Smith, *Science*, 2006, **312**, 1780–1782.
- P. Muhlschlegel, H. J. Eisler, O. J. F. Martin, B. Hecht and D. W. Pohl, *Science*, 2005, **308**, 1607–1609.
- M. E. Stewart, C. R. Anderton, L. B. Thompson, J. Maria, S. K. Gray, J. A. Rogers and R. G. Nuzzo, *Chem. Rev.*, 2008, **108**, 494–521.
- C. F. Bohren and D. R. Huffman, *Absorption and Scattering of Light by Small Particles*, Wiley, 1983.
- Z. C. Ruan and S. H. Fan, *Phys. Rev. Lett.*, 2010, **105**, 013901–013904.
- Z. C. Ruan and S. H. Fan, *Appl. Phys. Lett.*, 2011, **98**, 043101–043103.
- L. Verslegers, Z. F. Yu, Z. C. Ruan, P. B. Catrysse and S. H. Fan, *Phys. Rev. Lett.*, 2012, **108**, 083902–083906.
- F. Neubrech, A. Pucci, T. W. Cornelius, S. Karim, A. García-Etxarri and J. Aizpurua, *Phys. Rev. Lett.*, 2008, **101**, 157403–157406.
- U. Fano, *J. Opt. Soc. Am.*, 1941, **31**, 213–222.
- V. Giannini, G. Vecchi and J. G. Rivas, *Phys. Rev. Lett.*, 2010, **105**, 266801–266804.
- J. B. Lassiter, H. Sobhani, M. W. Knight, W. S. Mielczarek, P. Nordlander and N. J. Halas, *Nano Lett.*, 2012, **12**, 1058–1062.
- A. Christ, S. G. Tikhodeev, N. A. Gippius, J. Kuhl and H. Giessen, *Phys. Rev. Lett.*, 2003, **91**, 183901–183904.
- R. Adato, A. Artar, S. Erramilli and H. Altug, *Nano Lett.*, 2013, **13**, 2584–2591.
- R. Taubert, M. Hentsche, J. Kastel and H. Giessen, *Nano Lett.*, 2012, **12**, 1367–1371.
- A. Lovera, B. Gallinet, P. Nordlander and O. J. F. Martin, *ACS Nano*, 2013, **7**, 4527–4536.
- J. A. Fan, C. H. Wu, K. Bao, J. M. Bao, R. Bardhan, N. J. Halas, V. N. Manoharan, P. Nordlander, G. Shvets and F. Capasso, *Science*, 2010, **328**, 1135–1138.
- N. Verellen, Y. Sonnefraud, H. Sobhani, F. Hao, V. V. Moshchalkov, P. Van Dorpe, P. Nordlander and S. A. Maier, *Nano Lett.*, 2009, **9**, 1663–1667.
- F. Hao, P. Nordlander, Y. Sonnefraud, P. Van Dorpe and S. A. Maier, *ACS Nano*, 2009, **3**, 643–652.
- N. J. Halas, S. Lal, W.-S. Chang, S. Link and P. Nordlander, *Chem. Rev.*, 2011, **111**, 3913–3961.
- J. Ye, F. F. Wen, H. Sobhani, J. B. Lassiter, P. Van Dorpe, P. Nordlander and N. J. Halas, *Nano Lett.*, 2012, **12**, 1660–1667.
- C. Wu, A. B. Khanikaev, R. Adato, N. Arju, A. A. Yanik, H. Altug and G. Shvets, *Nat. Mater.*, 2012, **11**, 69–75.
- A. A. Yanik, A. E. Cetin, M. Huang, A. Artar, S. H. Mousavi, A. Khanikaev, J. H. Connor, G. Shvets and H. Altug, *Proc. Natl. Acad. Sci. U. S. A.*, 2011, **108**, 11784–11789.
- M. Rahmani, B. Luk'yanchuk and M. Hong, *Laser Photonics Rev.*, 2013, **7**, 329–349.
- A. E. Miroshnichenko, S. Flach and Y. S. Kivshar, *Rev. Mod. Phys.*, 2010, **82**, 2257–2298.
- B. Luk'yanchuk, N. I. Zheludev, S. A. Maier, N. J. Halas, P. Nordlander, H. Giessen and C. T. Chong, *Nat. Mater.*, 2010, **9**, 707–715.
- N. Liu and H. Giessen, *Angew. Chem., Int. Ed.*, 2010, **49**, 9838–9852.
- S. Sheikholeslami, Y. W. Jun, P. K. Jain and A. P. Alivisatos, *Nano Lett.*, 2010, **10**, 2655–2660.
- D. Dregely, M. Hentschel and H. Giessen, *ACS Nano*, 2011, **5**, 8202–8211.
- J. B. Lassiter, H. Sobhani, J. A. Fan, J. Kundu, F. Capasso, P. Nordlander and N. J. Halas, *Nano Lett.*, 2010, **10**, 3184–3189.
- C. P. Burrows and W. L. Barnes, *Opt. Express*, 2012, **18**, 3187–3198.
- S. Malynych and G. Chumanov, *J. Am. Chem. Soc.*, 2003, **125**, 2896–2898.
- A. D. M. C. L. Haynes, L. L. Zhao, R. P. Van Duyne, G. C. Schatz, L. Gunnarsson, J. Prikulis, B. Kasemo and M. Kall, *J. Phys. Chem. B*, 2003, **107**, 7337–7342.
- L. V. Brown, H. Sobhani, J. B. Lassiter, P. Nordlander and N. J. Halas, *ACS Nano*, 2010, **4**, 819–832.
- F. Hao, Y. Sonnefraud, P. Van Dorpe, S. A. Maier, N. J. Halas and P. Nordlander, *Nano Lett.*, 2008, **8**, 3983–3988.

- 36 S.-D. Liu, Z. Yang, R.-P. Liu and X.-Y. Li, *ACS Nano*, 2012, **6**, 6260–6271.
- 37 F. López-Tejeira, R. Paniagua-Domínguez, R. Rodríguez-Oliveros and J. A. Sánchez-Gil, *New J. Phys.*, 2012, **14**, 023035–023050.
- 38 F. López-Tejeira, R. Paniagua-Domínguez and J. A. Sánchez-Gil, *ACS Nano*, 2012, **6**, 8989–8996.
- 39 P. L. Stiles, J. A. Dieringer, N. C. Shah and R. R. Van Duyne, *Annu. Rev. Anal. Chem.*, 2008, **1**, 601–626.
- 40 B. Sharma, R. R. Frontiera, A.-I. Henry, E. Ringe and R. P. Van Duyne, *Mater. Today*, 2012, **15**, 16–25.
- 41 D. Cialla, A. Maerz, R. Boehme, F. Theil, K. Weber, M. Schmitt and J. Popp, *Anal. Bioanal. Chem.*, 2012, **403**, 27–54.
- 42 R. F. Aroca, D. J. Ross and C. Domingo, *Appl. Spectrosc.*, 2004, **58**, 324A–338A.
- 43 K. Ataka, T. Kottke and J. Heberle, *Angew. Chem., Int. Ed.*, 2010, **49**, 5416–5424.
- 44 I. A. Larmour and D. Graham, *Analyst*, 2011, **136**, 3831–3853.
- 45 J. R. Lakowicz, K. Ray, M. Chowdhury, H. Szmackinski, Y. Fu, J. Zhang and K. Nowaczyk, *Analyst*, 2008, **133**, 1308–1346.
- 46 Q. H. Wei, K. H. Su, S. Durant and X. Zhang, *Nano Lett.*, 2004, **4**, 1067–1071.
- 47 M. Pelton and G. W. Bryant, *Introduction to Metal-Nanoparticle Plasmonics*, Wiley, 2013.
- 48 E. C. Le Ru and P. G. Etchegoin, *Principles of Surface-Enhanced Raman Spectroscopy and Related Plasmonic Effects*, Elsevier, 1st edn, 2009.
- 49 T. H. Park and P. Nordlander, *Chem. Phys. Lett.*, 2009, **472**, 228–231.
- 50 S. Zhang, K. Bao, N. J. Halas, H. Xu and P. Nordlander, *Nano Lett.*, 2011, **11**, 1657–1663.
- 51 Y. Sonnefraud, A. Leen Koh, D. W. McComb and S. A. Maier, *Laser Photonics Rev.*, 2012, **6**, 277–295.
- 52 Y. S. Joe, A. M. Satanin and C. S. Kim, *Phys. Scr.*, 2006, **74**, 259–266.
- 53 S. Zhang, Z. Ye, Y. Wang, Y. Park, G. Bartal, M. Mrejen, X. Yin and X. Zhang, *Phys. Rev. Lett.*, 2012, **109**, 193902–193906.
- 54 N. Liu, L. Langguth, T. Weiss, J. Kastel, M. Fleischhauer, T. Pfau and H. Giessen, *Nat. Mater.*, 2009, **8**, 758–762.
- 55 C. L. G. Alzar, M. A. G. Martinez and P. Nussenzveig, *Am. J. Phys.*, 2002, **70**, 37–41.
- 56 R. Taubert, M. Hentschel, J. Kastel and H. Giessen, *Nano Lett.*, 2012, **12**, 1367–1371.
- 57 K. L. Kelly, E. Coronado, L. L. Zhao and G. C. Schatz, *J. Phys. Chem. B*, 2003, **107**, 668–677.
- 58 S. Nie and S. R. Emory, *Science*, 1997, **275**, 1102–1106.
- 59 M. Osawa, *Top. Appl. Phys.*, 2001, **81**, 163–187.
- 60 K. A. Willets and R. P. Van Duyne, *Annu. Rev. Phys. Chem.*, 2007, **58**, 267–297.
- 61 F. Hao, C. L. Nehl, J. H. Hafner and P. Nordlander, *Nano Lett.*, 2007, **7**, 729–732.
- 62 J. Nelayah, M. Kociak, O. Stephan, F. J. G. de Abajo, M. Tence, L. Henrard, D. Taverna, I. Pastoriza-Santos, L. M. Liz-Marzan and C. Colliex, *Nat. Phys.*, 2007, **3**, 348–353.
- 63 A. J. Haes, W. P. Hall, L. Chang, W. L. Klein and R. P. Van Duyne, *Nano Lett.*, 2004, **4**, 1029–1034.
- 64 A. J. Haes and R. P. Van Duyne, *J. Am. Chem. Soc.*, 2002, **124**, 10596–10604.